Available online at www.sciencedirect.com
SCIENCE DIRECT®
Materials Letters 60 (2006) 504–508
materials letters
www.elsevier.com/locate/matlet

Growth of ZnO thin film on SiO_2/Si substrate by pulsed laser deposition and study of their physical properties

M. Zerdali [a,*], S. Hamzaoui [a], F.H. Teherani [b], D. Rogers [b]

[a] *Laboratoire de Microscopie Electronique et des Sciences des Matériaux (LMESM), Université des Sciences et de Technologie d'Oran (USTO) BP1505 El M'Naouer, 31100, ORAN, Algerie, France*
[b] *Nanovation, 103, rue de Versailles, 91400 Orsay, France*

Received 25 June 2005; accepted 15 September 2005
Available online 14 October 2005

Abstract

Zinc oxide films were grown on SiO_2/Si substrate. The growths were performed using pulsed laser deposition at a moderate substrate temperature (500 °C). PLD ZnO/SiO_2/Si indicated a very well *c*-axis orientation. Micro-Raman and FTIR measurements were indicated vibrations modes of wurtzite structure and no evidence of defect density. Brillouin light scattering (BLS) measurements were performed to study the acoustic properties of ZnO films. A laser light source (514.5 nm) probe revealed acoustic phonons of about 300 nm wavelength. The BLS spectra revealed Rayleigh (R) and a number of guided Sezawa modes (S_i) in ZnO thin films. The S_i modes have high velocities and are polarised in the sagittal plane. Consequently, radio frequency (GHz) SAW devices could be fabricated using ZnO thin films on SiO_2/Si with great potential for use as SAW devices which can be readily integrated with Si-based semiconductor technology.

Keywords: ZnO; PLD; *C*-axis; Brillouin scattering; SAW

1. Introduction

Transparent conducting oxides, such as zinc oxide (ZnO), are of high technological relevance for applications such as flat panel displays for televisions and computers [1], for contacts on thin film photo-voltaics [2], and for energy efficient windows based on low infrared transmittance [3].

ZnO is also well-known as a piezoelectric material for use in surface acoustic wave (SAW) devices in delay lines, filters and resonators in wireless communications and signal processing [4]. Pulsed laser deposition (PLD) is a commonly used technique for the growth of ZnO thin films [5]. It has demonstrated its potential to produce highly oriented, well-crystallised films with low surface roughness, even on amorphous substrates.

Silicon oxide is a substrate of choice due to the potential for integration of acoustic elements with Si-based electronic circuitry [6]. An amorphous (SiO_2) interlayer is incorporated in the SAW device to operate as an insulator which suppresses the leakage current when a voltage is applied between the interdigit transducers (IDT). A similar approach is also adopted for transparent thin films transistors (TFT) [7], which can operate in the presence of a double-gate insulators consisting of SiO_2, and SiN_x.

In order to study the acoustic and elastic properties of the microstructure, it is necessary to fabricate an acoustic delay line [8], based on IDT [9]. In the GHz-band range, IDT are fabricated with sub-micron technology. This approach presents significant technical challenges for the investigation and detection of acoustic modes.

In this paper we report detailed study of the acoustic properties of ZnO thin films prepared by PLD. The study was conducted using a technique based on Brillouin Light Scattering (BLS) [10]. BLS has many advantages over conventional ultrasonic techniques commonly used for such studies [11], because it does not require external generation of acoustic waves, and because it probes acoustic phonons with wavelengths in the sub-micron range (0.2–0.4 μm): i.e. much shorter than those probed by ultrasonic methods. Moreover, use of a laser light source as a probe allows discrimination of acoustic phonons that are intrinsic to the bulk substrate material. Hence it

* Corresponding author. Tel./fax: +213 41 530460.
E-mail address: mokhtarzerdali@yahoo.com (M. Zerdali).

0167-577X/$ - see front matter © 2005 Published by Elsevier B.V.
doi:10.1016/j.matlet.2005.09.024

is possible to extract a larger amount of information from the films themselves.

A number of SAW modes confined within the film material can thus be revealed, namely the Rayleigh (R) [12], Sezawa (S_i) [13] and bulk modes (LM) [14,15]. Thus their corresponding velocities can be measured. This finding also implies that the PLD growth at moderate substrate temperature has yielded high quality ZnO films on SiO_2/Si.

These modes are promising for the development of novel, high-speed SAW devices operating in the GHz-band and which could be readily incorporated in semiconductor integrated circuitry.

2. Experimental details

An amorphous 150 nm thick SiO_2 layer was thermally grown on Si (001) substrate, characterized by a roughness (RMS) of ~0.30 nm. ZnO films were grown from a 99.9999% pure ZnO target by PLD using a KrF excimer laser (248 nm). The chamber was evacuated using a turbo-molecular pump to a background vacuum of about 1×10^{-7} Torr. The growth conditions were: a laser fluence of ~1.5 J/cm^2, laser frequency of 10 Hz, substrate temperature of ~500 °C, working partial pressure of molecular oxygen of $\sim1\times10^{-4}$ Torr, distance between the target and the substrate of ~50 mm and growth duration of 2 h.

Crystalline quality of ZnO films were investigated by a four circle goniometer (INEL) using a cobalt anode (CoK_α = 1.78897 Å) to detect (0002), (10$\bar{1}$1), and (10$\bar{1}$2) pole figures. The micro-Raman spectra were performed in backscattering configuration, using a 514.5 nm Ar^+ incident laser. The power was around 200 mW and the objective × 50. For infrared (IR) reflectance measurements, we used a Perkin Elmer FTIR GX spectrum with a KBr detector with 50 accumulations and a resolution of 1 cm^{-1}.

BLS measurements were performed at room temperature using a high sensitivity Sandercock-type 3+3 pass tandem Fabry–Perot spectrometer [16], characterized by a finesse of about 100 and a contrast ratio higher than 5×10^{10}. In this BLS experiment, a beam of monochromatic light of 100–500 mW p-polarised light was focused on the surface of the sample and used as a probe to reveal acoustic phonons of about 300 nm wavelength which are naturally present in the solid material. The power spectrum of these excitations was mapped out from frequency analysis of the light scattered for a given solid angle, by means of a multipass Fabry–Perot interferometer. The frequency-selected light transmitted by the interferometer was detected by a photomultiplier or an avalanche photodiode after passing through a second spatial filter for additional background suppression. A prism, or interference filter, between the second spatial filter and the detector, served to suppress inelastic light from common transmission orders outside the frequency region of interest. A computer collects the photon count levels and displays the data. The sampling time per spectrum is typically between 3 and 4 h.

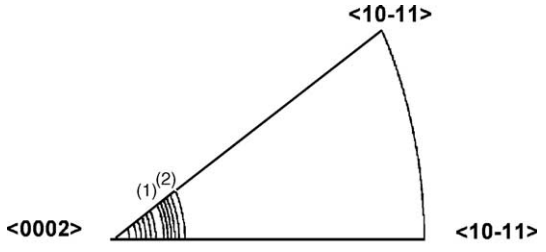

Fig. 1. Inverse pole figure of ZnO film grown at 500 °C and 10^{-4} Torr O_2 flow, along [0002]. The maximum intensity is equal to (1) 2147 cps, minimum (2) 0.0 cps.

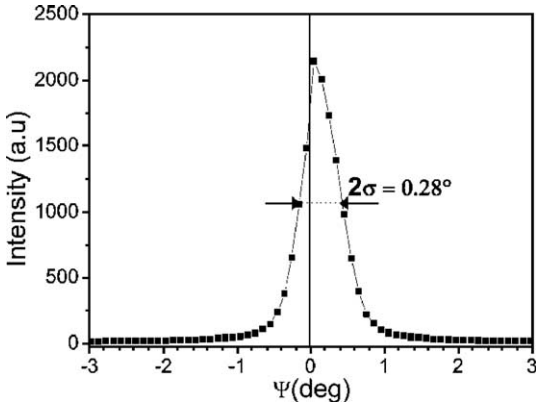

Fig. 2. Integrated intensity vs. Ψ-angle for determining c-axis orientation, the position of the peak intensity was at, Ψ=0.10°.

3. Results and discussions

3.1. X-ray diffraction

The orientation and crystalline structure of the ZnO film grown at 500 °C, is highly c-axis oriented, implying an alignment of the [0002] direction normal to the substrate plane.

Fig. 1 shows the (0002) inverse pole figure of the c-axis oriented ZnO film. The pole figure was obtained using the ZnO (0002) planes reflections (2θ=40.20°). The degree of the c-axis alignment normal to the substrate plane was indicated by the centering of the maximum intensity reflections from (0002) planes only around the azimuth angle, Ψ=0°. This result is evaluated through the fluctuation of the c-axis of the ZnO film around Ψ=0°. In Fig. 2 the integrated intensity of sample was estimated and plotted as a function of Ψ (deg). A deviation in the peak position of this curve from Ψ=0° represents the average

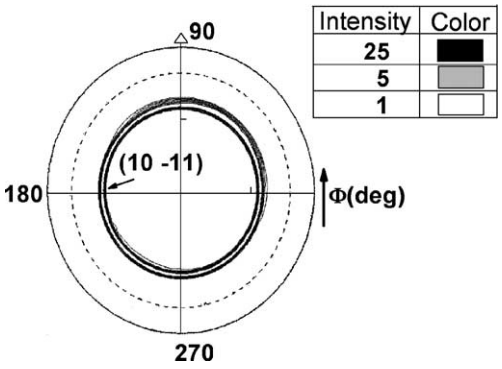

Fig. 3. Pole figure of ZnO film grown at 500 °C and 10^{-4} Torr O_2 flow, along [10$\bar{1}$1] using PLD. The maximum intensity is equal to (25) 18.97 cps, minimum (1) 0.0 cps. The ZnO film shows a fiber texture.

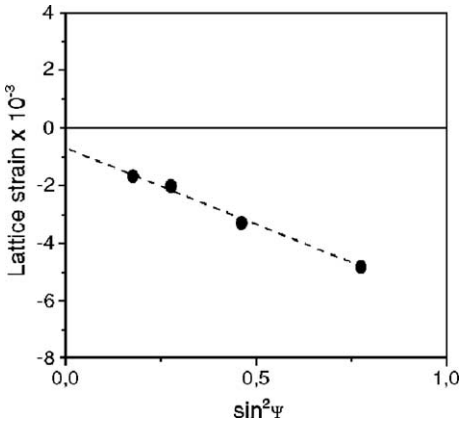

Fig. 4. The lattice strain of ZnO thin film prepared at 500 °C, and 10^{-4} Torr molecular oxygen flow. The linear distribution of the lattice strain is evident indicating a constant compressive stress.

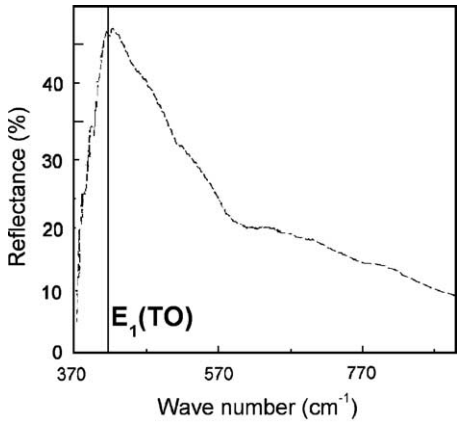

Fig. 5. FTIR spectrum for ZnO thin film indicating an absorbance band situated near 410 cm^{-1}, typical for ZnO wurtzite structure.

inclination of the *c*-axis from the surface normal. Doubled standard deviation 2σ of a Gaussian curve for the ZnO film was 0.28° and the average inclination (peak position) of the *c*-axis from the surface normal was within ±0.10°, in the aperture thickness of ~150 nm.

The degree of in-plane alignment in the films was further examined using the pole figure along [10$\bar{1}$1] orientation, obtained for 2θ=42.40° plane reflections. A ZnO crystal with a *c*-axis orientation possesses 6-fold symmetry. Thus, six poles should appear in the (10$\bar{1}$1) pole figure if it has a homogeneous in plane-alignment [17]. As is presented in Fig. 3, the observed ring indicates that the microstructure of ZnO films is columnar or fiber texture, but the *a*-axis of the hexagonal structure of the ZnO film is rotated randomly in the plane of the substrate. This is in agreement with the recent observations [18].

Our experimental condition was successfully chosen to form highly *c*-axis orientation even on amorphous substrate. The strong *c*-axis (0002) orientation of ZnO film can be analysed from energy minimization considerations [19]. The ZnO film will be formed with *c*-axis orientation by itself only if the growth condition is not deviated from optimum range of energetically stable state.

The lattice constants *c* (Å), and *a* (Å) were calculated from the position of (0004), (10$\bar{1}$4).

Both the measured values were 5.204 Å; 2θ=43.43°, and 3.229 Å; 2θ=49.30°, respectively. The lengths of the *c*-axis and *a*-axis were smaller than the powder lattice constants of ZnO used to evaluate the lattice strain for each diffraction lines. This implies that the film is under compressive stress induced by the growth process [20].

Fig. 4 shows the lattice strain for ZnO thin film recorded for the diffraction lines indicated in the Table 1. The evolution of the lattice strain is independent of an azimuth angle of a film surface, meaning that the strain distribution is on a $\sin^2 \Psi$. Linear distribution in a lattice strain relation to $\sin^2 \Psi_{hkl}$ is evident, indicating a constant compressive stress.

Table 1
Diffraction plane and relating parameters obtained with CoKα=1.78897 Å

hk1	2θ (deg)	Ψ_{hkl}	$\sin^2 \Psi_{hkl}$
10$\bar{1}$1	21.20	61.76	0.78
10$\bar{1}$2	28.00	42.95	0.47
10$\bar{1}$3	37.36	31.82	0.28
10$\bar{1}$4	49.30	24.96	0.18

3.2. Micro-Raman and FTIR spectroscopy

The infrared reflectance measurements were recorded for ZnO film on a normal incident light geometry (Fig. 5). The IR absorption spectra of ZnO film in the 350–750 cm^{-1} wave number range reveal the presence of an absorbance band situated at 410 cm^{-1}, which is attributed to the IR active E_1(TO) mode of wurtzite ZnO. This mode was attributed to the Zn–O stretching vibration for tetrahedral surrounding of zinc atoms [21]. This absorption band was closed to the recent IR reflectance measurements for ZnO films and for powder reference [18–22].

Fig. 6 shows the Raman band spectra which can be entirely explained on the basis of the published data for *c*-axis ZnO [23]. The E_2 (LO) mode is clearly seen at 437 cm^{-1}, typical for ZnO wurtzite structure. Whereas the E_1 (LO) mode around 579 cm^{-1} in the tail of the strong peak from silicon, is not evidenced. The E_1 (LO) peak was attributed to the formation of oxygen deficiency, interstitial Zn, and free carrier [24]. The E_2 (LO) peak intensity is strong dominant over E_1 (LO), and the absence of defect state of E_1 (LO) from our samples suggests a low defect density.

Additional peak is observed around 377 cm^{-1} recorded in Fig. 6, which was identified as A_1 (TO) mode [25]. The Raman scattering with A_1 (TO) modes indicates that the displacement of Zn^{+2} and O^{-2} ions is parallel to the *c*-axis, near the center of Brillouin zone (Γ point). The

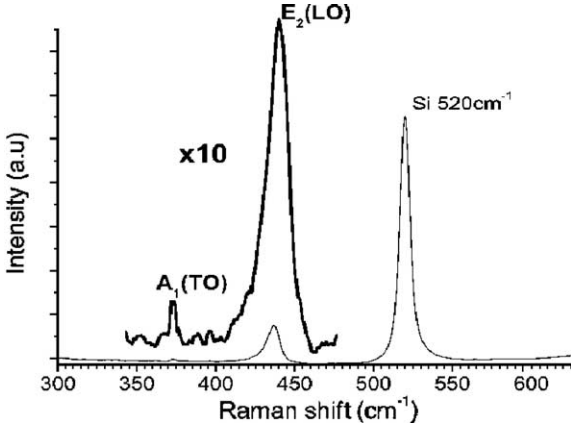

Fig. 6. Raman spectra for ZnO thin film grown on SiO2/Si substrate at 500 °C, and 10^{-4} Torr molecular oxygen flow. E_2 (LO) and A_1 (TO) modes are typical for ZnO wurtzite structure.

Table 2
Experimental values of the phase velocity of the different acoustic modes detected in BLS spectra

	V_R (ms^{-1})	V_{S1} (ms^{-1})	V_{S2} (ms^{-1})	V_{S3} (ms^{-1})
θ=55°	2669±50	3515±100	4500±100	5574±100
θ=65°	2626±50	3465±100	4409±100	–

ions move in the lattice with sufficiently high frequency but don't induce lattice deformation, while the presence of A_1 optical mode indicates the possibility of the presence of acoustic modes near the Γ point. The acoustic modes can be excited in piezoelectric material such ZnO at sufficiently lower frequency than A_1 (TO) [25]. This occurs only once the *c*-axis of ZnO film is highly oriented normally enough to the surface plane.

3.3. Brillouin spectroscopy and acoustic properties

In surface Brillouin scattering, SAW phonon is involved and the component of the wave-vector parallel to the surface is conserved.

In BLS spectroscopy, SAW phonons velocity V can be determined using the Debye approximation:

$$\Omega = Vq \tag{1}$$

where Ω, is the pulsation frequency of the acoustic wave (Hz), or phonon of wave vector q (m^{-1}) propagating with sound velocity V (ms^{-1}). The incident light with wave vector k_i and frequency ω_i, is scattered into a state k_S, ω_S such that:

$$\vec{k_s} = \vec{k_i} \pm \vec{q} \tag{2}$$

where the + sign to absorption (anti-Stokes process), and the − sign to emission (Stokes process) of the phonon. Correspondingly, the frequency is related by energy conservation:

$$\omega_s = \omega_i \pm \Omega. \tag{3}$$

The interaction geometry contributing to the inelastic scattering of the light from SAW phonons in the film is illustrated in Fig. 7, where k_i, k_S, k_t, and q are the incident, back scattering, transmitted photon, and SAW phonons wave vectors, respectively.

The SAW phonon phase velocity V is expressed from (Eq. (2)), as

$$V = \pi f / (k_i \sin(\theta)) \tag{4}$$

where θ, is the orientation of the incident light with respect to the normal surface, for plane incidence and f (Hz), the frequency value of the SAW mode.

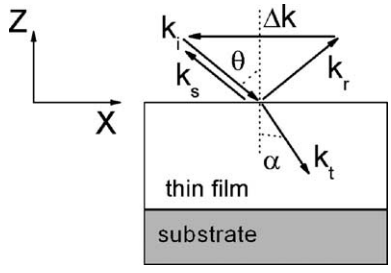

Fig. 7. Scattering geometries used in the present study. k_i, k_r, k_s, k_t, and q, are incident, reflected, backscattered, transmitted photon, and surface phonon wave vectors, respectively.

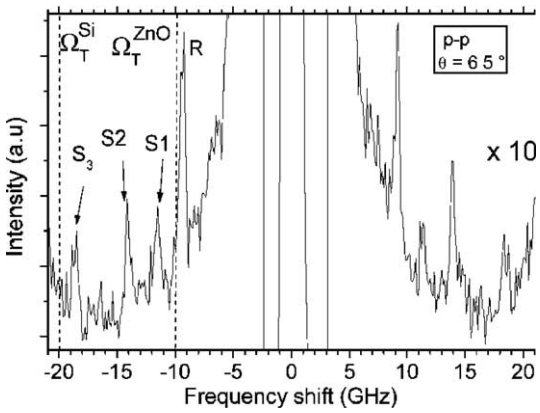

Fig. 8. p–p Brillouin spectrum from ZnO/SiO2/Si, taken at an angle of incidence, θ, of 65°. Ω_T^{ZnO}, Ω_T^{Si} is the transversal threshold frequency of ZnO layer and Si substrate.

We note that for a fixed value of SAW velocity, the experimentally obtained frequency Ω (phonon) is dependent on the incident light angle, θ.

Measurements performed in the p–p configuration enabled us to observe a sequence of representative spectra, as shown in Fig. 8.

We performed BLS measurements at different angles of incidence θ=45°, 55° and 65° in order to identify SAW modes (Table 2). For all spectra we could readily distinguish the variation with θ of three or four well-defined surfaces modes. The surface mode is identified according to their frequency position relative to the transverse Ω_T and to the longitudinal Ω_L threshold frequency. For the (R) mode, we have, $\Omega_R < \Omega_T^{(film)}$. Notice that ($S_i$) guided mode frequencies (Ω_S) are bounded by the transverse frequencies of the phonons in the film and of the phonons in the substrate:

$$\Omega_T^{(film)} < \Omega_s < \Omega_T^{(substrate)}. \tag{5}$$

In Fig. 7, the more intense peak, located at lower frequency (≈9 GHz), corresponds to the (R) mode in the ZnO layer, while the following lower-intensity peaks, labelled (S_i), are due to the first, second and the third Sezawa modes. The (R) and (S_i) SAW modes are observed in all spectra. The (R) SAW is an evanescent mode, and has a sagittal polarisation, as do the (S_i) modes.

This leads to the characteristic profiles of the amplitudes of the displacements (u_x, u_z) for the (R) and (S_i) modes represented in Fig. 8. In this figure one can recognise the main characteristic features as: an exponential damping profile for the (R) mode surface and an oscillating profile for the (S_i) guided modes in the ZnO layer. The Sezawa modes vanish i times in the ZnO layer and decay exponentially in the substrate.

Measurements of the frequency position of these Brillouin peaks provide us with the phase velocities V of the corresponding SAW modes, according to the Eq. (4). Notice that the phase velocity of the R-SAW is $\beta\sqrt{(C_{44}/\rho)}$, where $\beta \approx 0.94$ is only weakly dependent on elastics constants C_{11}, C_{13}, and C_{33}. Hence elastic constant C_{44} can be determined directly if we have knowledge of the mass density ρ of the ZnO (5676 Kg/m^3) [26].

4. Conclusion

BLS measurements were used to study the acoustic properties of ZnO thin films. The ZnO films were grown on SiO_2/Si substrates using PLD at a moderate substrate

temperature (500 °C). Highly *c*-axis oriented was obtained normal to the substrate surface plane. The IR measurements indicate the no evidence of defect density and the strong peak intensity of E_2(LO) mode, typical for wurtzite structure.

As well as a Rayleigh (R) mode and a number of Sezawa (S_i) guided acoustic modes polarised in the sagittal plane, travelling parallel to the free surface.

Based on this finding it can be proposed that GHz-band SAW devices could be fabricated using ZnO thin films and ULSI technology. This work shows that PLD growth at relatively low substrate temperature can be used to grow high quality ZnO SAW films on SiO_2/Si. Such films could be of great importance for incorporation of SAW in Si-based integrated circuitry.

References

[1] D.C. Reynolds, D.C. Look, B. Jogai, H. Mokoe, Solid State Commun. 101 (1997) 643.
[2] C.H. Parck, I.S. Jeong, J.H. Kim, S. Im, Appl. Phys. Lett. 82 (22) (2003) 3974.
[3] Rajesh Das, Swati Ray, J. Phys., D, Appl. Phys. 36 (2003) 152–155.
[4] P.S. Smith, C.K. Campbell, IEEE Trans. On Ultrasonics, Ferroelectrics, and Frequency Control 36 (1) (1989) 13.
[5] T. Ohshima, R.K. Thareja, T. Ikgami, K. Ebihara, Surf. Coat. Technol. (2003) 169–170.
[6] S. Mthukumar, C.R. Gorla, V.W. Emametoglu, S. Liang, Y. Lu, J. Crystal Growth 225 (2001) 197.
[7] S. Masuda, K. Kitamura, Y. Okumura, S. Miyatake, H. Tabata, T. Kawai, J. Appl. Phys. 93 (3) (2003) 12625.
[8] I. Tseng Tang, H.J. Chen, W.C. Hwang, M.P. Houng, J. Crystal Growth 262 (2004) 464.
[9] H. Matthews, Surface Acoustic Filter, Wiley, New York, 1977.
[10] X. Zhang, J.D. Comin, A.G. Every, T.E. Deriy, Phys. Rev., B. 65 (2001) 012106–012111.
[11] G. Carlotti, G. Socino, A. Ptri, E. Verona, Appl. Phys. Lett. 51 (23) (1987) 1889.
[12] V. Panella, G. Carlotti, G. Socino, L. Giovannini, M. Eddrief, C. Sebenne, J. Phys. Condens. Matter 11 (1999) 6667.
[13] G.W. Farnell, E.L. Adler, in: W.P. Mason, R.N. Thurston (Eds.), Physical Acoustics, For a Review of Acoustic Modes in a Thin Film, vol. 9, Academic, New York, 1972.
[14] G. Carlotti, G. Gubbiotti, F.S. Hickernell, H.M. Liaw, G. Socino, Thin Solid Films 310 (1997) 36.
[15] F. Nizzoli, J.R. Sandercock, in: G.R. Horton, A.A. Mradudin (Eds.), Dynamical Properties of Solids, vol. 6, North-Holland, Amsterdam, 1990, p. 307.
[16] J.R. Dutcher, S. Lee, J. Kim, G.I. Stegeman, C.M. Falco, Phys. Rev. Lett. 65 (1990) 1231.
[17] K. Matsubra, P. Fons, A. Yamada, M. Watanabe, S. Niki, Thin Solid Films 347 (1999) 238–240.
[18] Rong-Ping wang, Hachizo Muto, Takeshi Kusumori, Opt. Mater. (2003) 1–6.
[19] N. Fujimura, T. Nishihara, S. Goto, T. Xu, J. Ito, J. Crystal Growth 130 (1993) 633.
[20] Takao Hanabusa, Hiroyoshi Hosoda, Kazuya Kusaka, Kikuo Tominaga. Thin Solid Films. 343–344 (199) 164–167.
[21] E.M. Bachari, G. Baud, S. Ben Amor, M. Jacquet, Thin Solid Films 348 (1999) 165–172.
[22] M. Tzolov, N-Tzenov, D. Dimova-Malinovska, M. Kalitzova, C. Fizzuto, G. Vitali, G. Zollo, I. Ivanov, Thin Solid Films 379 (2000) 28–36.
[23] T.C. Damen, S.P.S. Porto, B. Tell, Phys. Rev. 142 (1966) 570.
[24] J. Nan Zeng, Juay Kiang Low, Zhong Min Reu, Thomas Liew, Yong Feng Lu, Appl. Surf. Sci. 8027 (2002) 1–6.
[25] Toshio Kamiya, Jpn. J. Appl. Phys 35 (1996) 4421–4426.
[26] T. Azuhatu, M. Takesada, T. Yagi, A. Shikanai, S.F. Chichibu, K. Torii, A. Nakamura, T. Sota, G. Cantwell, D.B. Eason, C.W. Litton, J. Appl. Phys. 94 (2) (2003) 970.